

Injection current ferroelectric in group IV-monochalcogenide monolayers

Suman Raj Panday,¹ Salvador Barraza-Lopez,² Tonatiuh Rangel,³ and Benjamin M. Fregoso¹

¹Department of Physics, Kent State University, Kent OH, 44242, USA

²Department of Physics, University of Arkansas, Fayetteville AR, 72701, USA

³Department of Physics, University of California, Berkeley CA, 94720, USA

Group-IV monochalcogenide (GeS, GeSe, SnS, SnSe) monolayers are two-dimensional ferroelectrics predicted to produce large shift currents and second harmonic generation. Using density functional theory methods, we show that these materials also exhibit a large injection current (also known as the circular photogalvanic effect). Injection current can reach values up to 10^{11} A/V²s in the visible spectrum; two orders of magnitude larger than its magnitude in the prototypical nonlinear semiconductor CdS. We discuss the correlations between injection current, the electronic density of states and the electric polarization. We show that the absolute value of the short-circuit frequency-*average* injection current is transverse to and correlated with the spontaneous electric polarization, but not correlated with the density of states. Our results establish GeS, GeSe, SnS, SnSe monolayers as versatile nonlinear materials suitable for optoelectronic applications in two-dimensions.

I. INTRODUCTION

The nonlinear optical response of materials is of fundamental importance for basic and applied research. Effects such as the shift and injection currents have been theoretically and experimentally explored since the 1970's.¹ They have attracted a lot of attention in the last few years for their potential applications in novel optoelectronic devices, including solar photovoltaic cells whose efficiency is not limited by the Shockley-Queisser limit.²

The shift and injection currents differ from conventional pn-junction-based photovoltaic mechanisms in that the former require no potential barriers or interfaces, homogeneous materials without an inversion center can generate large injection or shift photocurrents upon illumination. The injection current can be understood as an asymmetric injection of charge carriers into time-reversed k -points in the first Brillouin zone (BZ), which creates a polar distribution and hence a current. This current varies linearly with time, in the absence of momentum relaxation and saturation effects. The injection current has been observed in CdS³, CdSe,³ and many other materials.

Of great interest is the nonlinear optical response of two-dimensional (2D) materials⁴ such as GeSe, GeS, SnSe and SnS monolayers, henceforth referred collectively as group-IV monochalcogenide monolayers⁵⁻⁸ (MMs). Recent numerical work predicts these materials exhibit a very large second harmonic generation^{7,8} (SHG) and shift current⁶ despite them being only a few Angstrom thick. Experimental confirmation is underway, with Titova reporting large terahertz radiation in few-layer GeS that is consistent with shift current generation.⁵ Interestingly, at temperatures below a critical temperature T_c (*e.g.*, Refs. 9–11) MMs are 2D ferroelectrics too, thus providing a two-dimensional playground to investigate the relation between their nonlinear optical response and electric polarization.

Rappe and coworkers showed that there is no general relationship between spontaneous electric polariza-

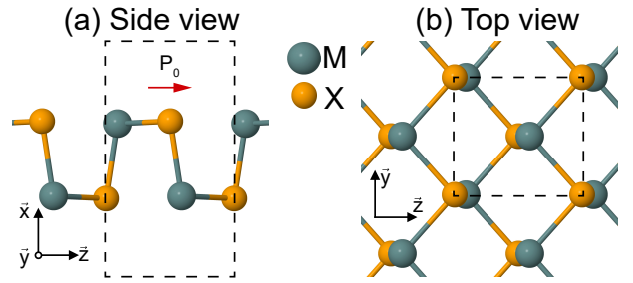


FIG. 1. Structure of monochalcogenide monolayers (MMs); M=Ge,Sn X=S,Se. The unit cell contains 4 atoms and is indicated within boxes. The space group lacks an inversion center and develops a nonzero in-plane spontaneous polarization P_0 .

tion and shift current in bulk three dimensional (3D) ferroelectrics.¹² Nevertheless, the strong covalent bonds formed by states involved in the transition and the large asymmetry of the wavefunction were identified as two important factors determining the magnitude of the shift current.¹² Some peaks in the imaginary part of the dielectric function, whose frequency dependence follows the joint density of density of states (JDOS), seem to coincide with those of the shift current. These strong absorption peaks should then explain the large optical response. However, much structure is missed, making the shift current more sensitive to the Bloch wavefunctions than to the band structure.

We have shown that the shift current in MMs is roughly proportional to band-polarization differences and hence, other things being equal, good ferroelectrics will produce large shift photocurrents.^{6,13} In fact, the shift current along the polar axis can be modeled in terms of stacked one-dimensional ferroelectric chains. A similar situation arises for the second harmonic generation of MMs. A very large response is obtained, which is proportional to the shift current tensor in a two-band model.⁷

In this paper, we now study the magnitude and direction of the injection current on GeSe, GeS, SnSe and SnS monolayers. We also investigate its correlation with

the JDOS and the spontaneous polarization P_0 . Using a simple tight-binding model, we explore its microscopic origin. Similar to the shift current, we find a large injection current; two orders of magnitude larger than that of the prototypical semiconductor CdS³. Given the similarities between the injection current expression and the imaginary part of the dielectric function, we expected the JDOS to be correlated to the injection current, but found this not to be the case. Surprisingly, the frequency-average injection current is correlated with the spontaneous electric polarization in a way similar the frequency-average of shift current is correlated to the polarization⁶. These results imply that both shift current *and* injection current strongly depend on the form of the Bloch wavefunction, and not just on the band structure. In addition, we determine an optimal value of polarization, which gives the maximum injection current.

II. METHODS

We use density functional theory (DFT) as implemented in the ABINIT¹⁴ computer package, with the generalized gradient approximation to the exchange correlation energy functional as implemented by Perdew, Burke and Ernzerhof.¹⁵ Hartwigsen-Goedecker-Hutter norm conserving pseudo potentials¹⁶ were employed. To expand the plane waves basis set, energy cutoffs of 50 Hartrees were employed for GeS and GeSe, and 60 Hartrees for SnS and SnSe. We set a separation of 15 Å along the x -direction in Fig. 1, which makes for more than 10 Å of vacuum among periodic images. To calculate the injection current, we included 20 valence and 30 conduction bands for GeS and SnS, and 30 valence and 20 conduction bands for GeSe and SnSe. They account for all allowed transitions up to 6 eV. We also used a mesh of 70×70 k -points along the y - and z -directions in Fig. 1.

To extract the effective response of a monolayer, we factor the response per unit length perpendicular to the slab and multiply it by an effective thickness. The procedure amounts to scale the numerical results by a factor L/d , where L is the super cell lattice parameter perpendicular to the slab, and d is the effective thickness of the monolayer. Here, we use effective slab thicknesses of 2.560, 2.593, 2.849 and 2.758 Å for GeS, GeSe, SnS, and SnSe, respectively. Once the ground-state wave function and energies were computed, the TINIBA package¹⁷ was used to compute the injection current susceptibility η_2^{abc} as implemented in Ref. 18. The sum over k -points is made using the interpolation tetrahedron method.¹⁹ See the Appendices for more details.

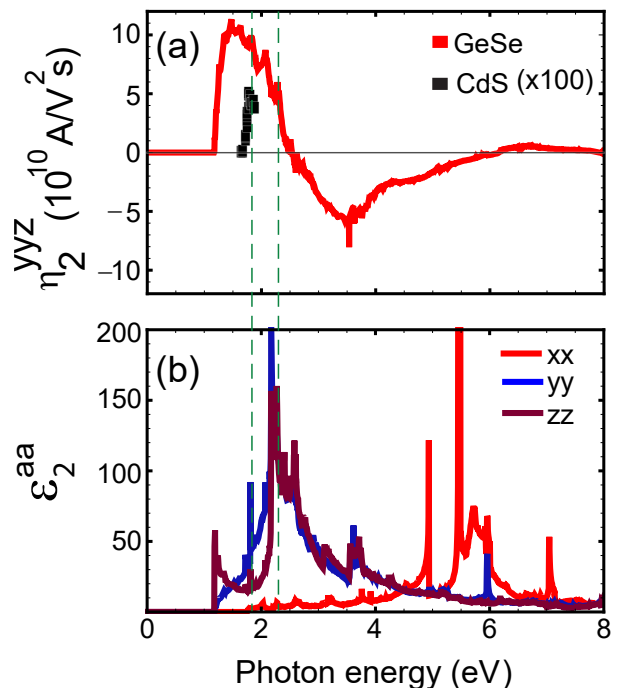


FIG. 2. (a) Imaginary part of the nonzero injection current tensor for GeSe (red line). Experimental values for CdS are shown by black squares, and multiplied by 100 to make them visible³. (b) Imaginary part of the dielectric function, ϵ_2^{aa} from Eq. 3.

III. RESULTS

A. Injection current

An incident monochromatic optical field $E^a = E^a(\omega)e^{-i\omega t} + \text{c.c.}$ induces an injection current governed by the equation¹⁸

$$\frac{d}{dt} J_{inj} = 2\eta_2^{abc} E^b(\omega) E^c(-\omega) - \frac{J_{inj}}{\tau}. \quad (1)$$

τ is a phenomenological momentum relaxation time and $\eta_2^{abc}(0, \omega, -\omega)$ is the injection current tensor

$$\eta_2^{abc} = \frac{e^3 \pi}{2\hbar^2 V} \sum_{nmk} \omega_{mn,a} f_{nm} [r_{mn}^c, r_{nm}^b] \delta(\omega_{mn} - \omega), \quad (2)$$

where $a, b, c = x, y, z$ are Cartesian components, n is the band index, $f_{nm} = f_n - f_m$ is the difference in occupation numbers at zero temperature of bands n and m , $\hbar\omega_n$ is the energy of the band n , $r_{nm}^a = i\langle u_n | \nabla^a | u_m \rangle$ are the Berry connections, $[r_{mn}^c, r_{nm}^b] = r_{mn}^c r_{nm}^b - r_{mn}^b r_{nm}^c$, and summation over repeated indices is implied. We define the subscript $,a$ to mean a crystal momentum derivative with respect to Cartesian index a , i.e., $X_{,a} = \partial X / \partial k_a$ and hence $\omega_{nm,a} \equiv \omega_{n,a} - \omega_{m,a} = v_n^a - v_m^a$ are band-velocity differences.

η_2^{abc} is a purely imaginary third rank tensor which is antisymmetric in the last two indices. It vanishes for

linearly polarized light, and this is why the effect we are describing receives the alternative name of a circular photogalvanic effect. With a point group of $mm2$, MMs lack a center of inversion. Hence, the nonzero components of this tensor are zxx , zyy , zzz , yyz , xzx , xxz and yzx . Antisymmetry of η_2 with respect to exchange of the last two indices implies that the zxx , zyy , zzz components vanish. There are two independent components out of the four remaining ones. With the notation set in Fig. 1 in which the x -direction separates periodic images, the in-plane component yyz becomes the focus of this paper, the other independent component being vanishingly small. Importantly, only injection current flow *transverse* to the polarization \mathbf{P}_0 is allowed.

We show in Fig. 2(a) the injection current for the GeSe monolayer as a function of the phonon energy, $\hbar\omega$. The response of other materials is similar and presented in Appendix B. The first thing to notice is the maximum of the injection current, which reaches a value as large as 10^{11} A/V²s in the visible range. To give perspective of this value, the measured injection current of the prototypical semiconductor CdS is two orders of magnitude smaller³, highlighting the actual potential of MMs for optoelectronic applications. As the photon energy increases the injection reverses direction several times and progressively decreases in magnitude.

In order to understand the origin of the large injection current, we first compare it to the imaginary part of the linear dielectric function

$$\varepsilon_2^{ab} = \frac{e^2\pi}{\varepsilon_0\hbar V} \sum_{nm\mathbf{k}} f_{nm} r_{nm}^a r_{mn}^b \delta(\omega_{mn} - \omega), \quad (3)$$

whose frequency dependence follows the JDOS. Our linear response calculation, shown in Fig. 2(b), agrees with previous reports.^{6,20} Higher ε_2 leads to higher absorption rates in particular near the van Hove peaks. Inspection of Fig. 2(b) shows that only few peaks in the injection current match the energy locations of van Hove singularities in ε_2 (two of them indicated by dashed vertical lines). There appears to be no one to one relation between the magnitude nor direction of the injection current and ε_2 . We therefore conclude that the form of the Bloch wave functions is playing a significant role on the magnitude of the injection current.

B. Average injection current *versus* spontaneous polarization

The shift current defines a gauge-invariant length scale (the so-called shift vector), which can naïvely be associated with the length of the microscopic dipole in ferroelectric materials. One would then expect the shift current in ferroelectrics to correlate with the ferroelectric order parameter P . This turns out not to be the case in bulk ferroelectrics.¹² In 2D, however, the shift current expression can be shown to depend on band-polarization

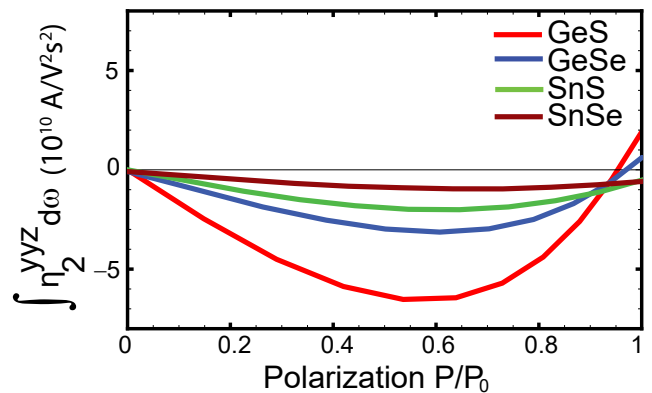


FIG. 3. Frequency-integral of the imaginary part of the injection current tensor vs. polarization for all single-layer MMs. The integral is proportional to the *average* injection current generated under illumination by a frequency-independent (white) light source. The polarization is calculated along a path connecting the symmetric ($P = 0$) and asymmetric (ground state with $P = P_0$) configurations. The average current is nonmonotonic, with an optimal value of P yielding maximal photocurrent.

differences, so that it correlates with the ferroelectric order parameter.⁶

The injection current, on the other hand, does not define an intrinsic length scale and hence one should not expect correlations with P . To our surprise, the injection current does appear to be correlated with P in MMs. To be precise, we consider a circularly polarized optical field incident perpendicular to the plane defined by the GeSe monolayer. From Eq. 1 we have

$$\frac{d}{dt} J_{inj}^y = \pm 4i\eta_2^{yyz} |E_0(\omega)|^2 - J_{inj}^y/\tau, \quad (4)$$

where \pm is determined the chirality of light and $E_0(\omega)$ is the amplitude of the optical field. The injection current becomes $J_{inj}^y = \pm 4\tau i\eta_2^{yyz} |E_0(\omega)|^2$ in steady state. If the light has a flat spectrum, the frequency-average current is its sum over all frequencies divided by the bandwidth $\Delta\omega = (W - E_g)/\hbar$

$$J_{inj,avg}^y = \pm 4i\tau |E_0|^2 \frac{1}{\Delta\omega} \int_0^{W/\hbar} d\omega \eta_2^{yyz}. \quad (5)$$

Hence, the average injection current is proportional to the frequency-integral of the injection current tensor. W is about 6 eV in practice. Alternatively, if τ is small enough the injection current will follow the envelope of an incident optical pulse and $-i\tau\eta_2^{yyz}$ can be interpreted as an effective (injection) current in ultrafast (ps) pulsed experiments.

The spontaneous polarization^{21,22} is calculated along a minimal-energy path from the asymmetric ground state configuration to the centrosymmetric state configuration,

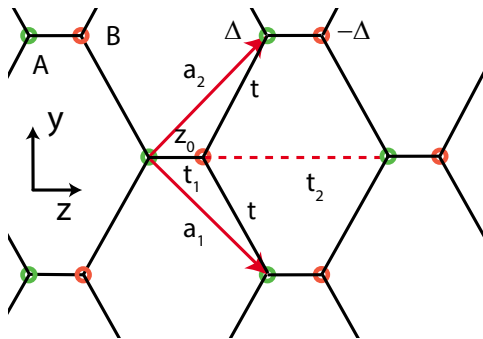


FIG. 4. Geometry of the two-band model for GeSe. The lattice has two nonequivalent lattice sites (A, B) (a distance z_0 apart) per unit cell, and lattice vectors $\mathbf{a}_1, \mathbf{a}_2$. Nearest and next-to-nearest neighbors are taken into account. The crystal lacks inversion symmetry and a spontaneous polarization develops along the z axis.

both in the rectangular unit cell, as implemented in the ABINIT code.¹⁴ Barring pathologies, the system is expected to transition via domain wall motion through a unique path in phase space under a constant area constraint.¹¹ We take the path to be straight lines with minimal error.⁶ The lines are parametrized by λ , each atomic position given by $\mathbf{R}^i(\lambda) = \mathbf{R}_0^i + \lambda(\mathbf{R}_f^i - \mathbf{R}_0^i)$, where \mathbf{R}_0^i (\mathbf{R}_f^i) is the initial (final) position of atom i in the centrosymmetric (noncentrosymmetric) structure. Our polarization values agrees with reports that follow a similar area constraint,^{6,23} see Appendix C for more details.

Fig. 3 shows the frequency-integral of the injection current tensor as a function of P for all MMs. The result implies that the *average* injection current is a nonmonotonic function of the P for all studied materials. The material with the largest spontaneous polarization (GeS)⁶ gives the largest absolute average injection current. There is an optimal value of P for which a maximum injection current is obtained. Our results suggest a way to engineer the injection current in MMs by applying stress to the crystal.

C. Direction of the injection current in GeSe

Finally, we investigate the origin of the direction changes in the injection current, Fig. 2a, using a minimal two-band microscopic model of GeSe. The point is to find the key parameter(s) which reproduce, if not the details of the frequency dependence, the sign change. The geometry of simplest two-band model for GeSe is shown in Fig. 4. We include onsite potentials $\pm\Delta$ at (A, B) sites, next nearest neighbors t, t_1, t_2 and next-to-nearest neighbors t_{AA}, t_{BB} . Further details of the model are presented in Appendix D.

We find that it is necessary for the model to have next-nearest neighbor interaction to reproduce the sign change

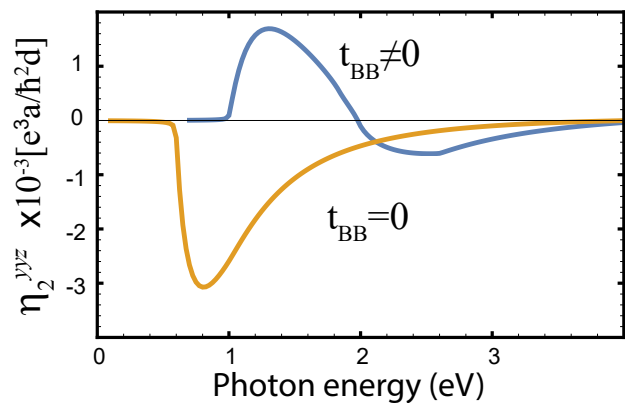


FIG. 5. Injection current in the two-band model for two values of the hopping between B-sites t_{BB} . The injection current flips sign only when there is non-zero Ge-Ge or Se-Se hopping terms. The parameters used are $t = .5$ eV, $t_1 = .3$ eV, $t_2 = .7$ eV, $\Delta = .3$ eV, $t_{AA} = 0$, $t_{BB} = .5, 0$, $z_0 = a$, $\mathbf{a}_1 = (a, -a)$, $\mathbf{a}_2 = (a, a)$ with a the lattice parameter.

in η_2 , see Fig. 5. This suggests Ge-Ge and Se-Se interactions are responsible for the oscillatory sign changes of the injection current in GeSe.

IV. EXPERIMENTAL SIGNATURES

Injection current can be detected under continuous illumination with electrodes connected to the sample^{24–28} or by spectroscopy of the THz emission following a (ps) pulse^{24–28}. In either we require light with circular polarization and expect the current to flow perpendicular to the polarization vector of the material.

The macroscopic injection current flowing in a the sample requires acknowledge of the momentum relaxation mechanisms. A simple relaxation time approximation can give an order of magnitude estimate. Typical momentum relaxation times of MMs are 100 fs (see Ref. 29 and standard field amplitudes are $E_0 \sim 10^6$ V/m. The expected injection current $|J_{inj}| \sim -4i\tau\eta_2^{yyz}|E_0|^2$ per unit of incident intensity $I = 2ce|E_0|^2$ is estimated to be $J_{inj}/I \sim 300\text{mA/W}$, where we used $\eta_2^{yyz} \sim 10^{11}$ A/V²s (Fig. 2a) at peak and 50 for the dielectric constant see Fig. 2b. This value is easily detected and should be compared with state-of-the art silicon-based solar cells 400 mA/W³⁰.

V. CONCLUSIONS

Understanding the nonlinear optical response of solids is of fundamental importance for novel optoelectronic applications of novel two-dimensional ferroelectric materials. Here, we studied the injection current of ferroelectric GeSe, GeS, SnS and SnSe monolayers, which have been predicted to exhibit large nonlinear optical re-

TABLE I. Band gaps and effective 3D polarization of single-layer MMs within DFT-PBE.

Monolayer	Direct gap <i>eV</i>	Indirect gap <i>eV</i>	Polarization <i>C/m²</i>
GeS	2.13	1.71	1.948
GeSe	1.12	1.12	1.372
SnS	1.49	1.36	0.954
SnSe	0.82	0.82	0.719

sponses such as shift current and second harmonic generation. We calculated the injection current and investigated its magnitude, direction and correlations with the density of states and the electric polarization.

The injection current is very large in the visible regime, much larger than in prototypical semiconductors and comparable to the shift current⁶. The density of states is not correlated to (nor is a good predictor of) the injection current, despite the naïve expectation that band structure effects dominate it. Second, the short-circuit frequency-average injection current correlates with the spontaneous polarization. Materials with a larger spontaneous polarization have larger absolute average injection current, and an optimal value of P which yields maximum current. The direction change of the injection current with frequency of incident light is due to the Ge-Ge or Se-Se electronic interaction. Our findings establish GeSe, GeS, SnS and SnSe monolayers as excellent nonlinear optical materials for future optoelectronic applications.

VI. ACKNOWLEDGMENTS

We thank the U.S. Department of Energy, Office of Basic Energy Sciences, Early Career Award DE-SC0016139 and Contract No. DE-AC02-05CH11231.

Appendix A: Electronic bandstructures

The electronic band structures calculated within DFT are shown in Fig. 6; they agree with previous works.³¹ For each material, the DFT bandgap E_g is indicated in the figure and in Table I.

Appendix B: Linear and injection current spectra

We used TINIBA to obtain the injection current curves. Convergence was achieved with a 70×70 k -point mesh, see Fig. 8. In Fig. 7, we show the non negligible injection current tensor component, η_2^{yyz} for GeSe, GeS, SnS and SnSe monolayers. In all materials, we see a very large response (up to 10^{11} AV²/s). We also show

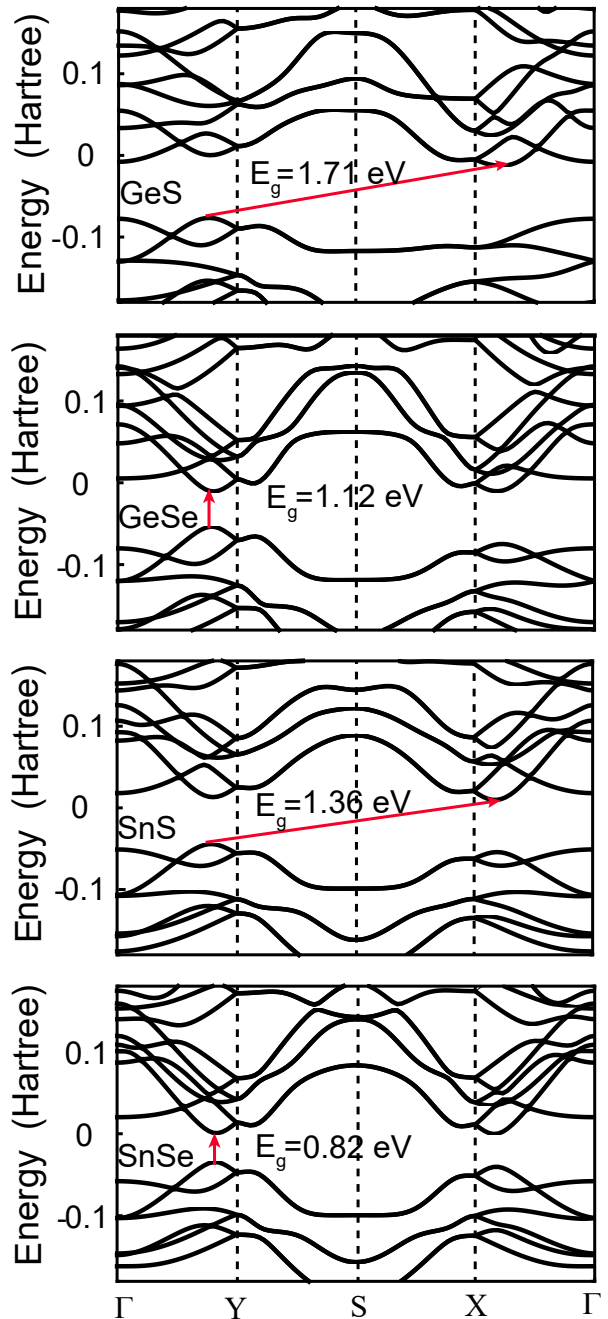


FIG. 6. Electronic bandstructure of MMs calculated within DFT-PBE. The k -point path along the first Brillouin zone chosen is shown at the bottom, and the bandgaps are shown in units of eV.

the imaginary part of the dielectric function, whose frequency dependence is essentially given by the JDOS and it controls the linear optical absorption. Close inspection reveals that only few peaks in ϵ_2 correspond to peaks in η_2 (as indicated by dashed lines) and in general, there is no visible relation with the injection current.

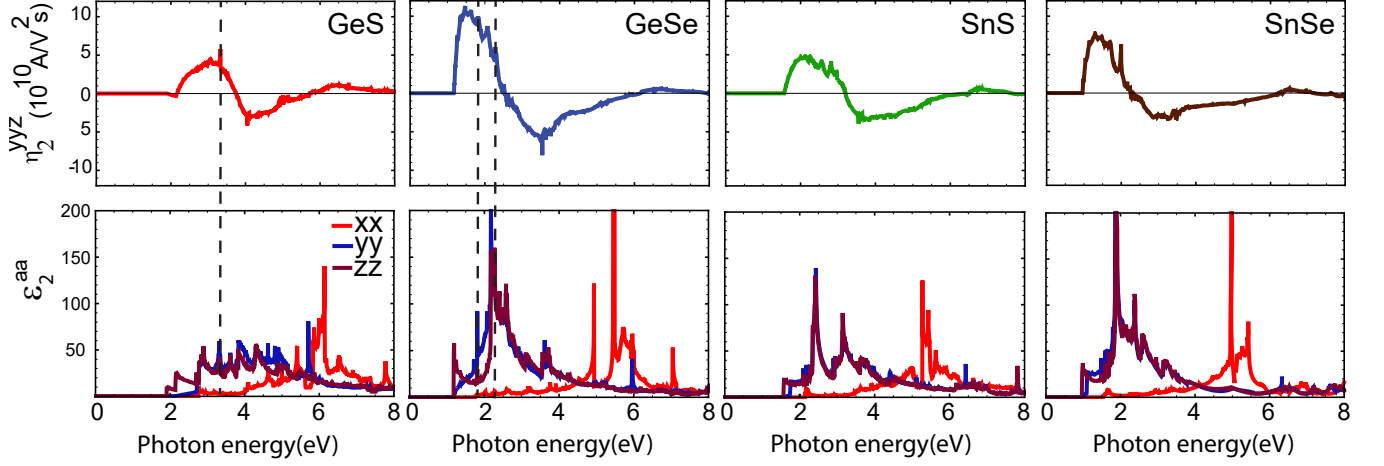


FIG. 7. (top panels) Imaginary part of the injection current tensor of group-IV monochalcogenides monolayers. For comparison we also show the imaginary part of the linear dielectric function ϵ_2 (bottom panels), whose frequency dependence follows the joint density of states (JDOS) and determines the linear optical absorption. As can be seen there is no correlation between the two and injection current depends on the form of the Bloch wave function.

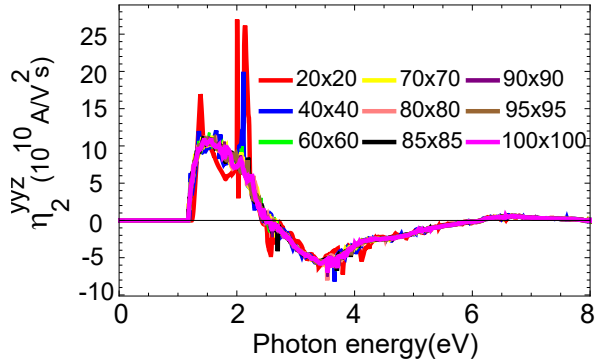


FIG. 8. Convergence of the injection current tensor for GeSe monolayer with respect to the k -point mesh size.

Appendix C: Electric polarization and injection current

We calculate the spontaneous polarization as implemented in ABINIT using the following expression:

$$P^a(\lambda) = \frac{e}{V} \sum_i Z^i r_i^a(\lambda) - \frac{ie}{V} \sum_{\mathbf{v}\mathbf{k}} \langle u_{\mathbf{v}}^\lambda | \nabla^a | u_{\mathbf{v}}^\lambda \rangle, \quad (\text{C1})$$

where $u_{\mathbf{v}}^\lambda$ are Bloch wave functions, Z^i is the atomic number of the i th atom, and V is the simulation volume. λ parameterizes an adiabatic path from a centrosymmetric configuration to the ground-state configuration. The polarization is defined as the difference between the polarization of two smoothly connected atomic structures: \mathbf{R}_0^i with inversion symmetry (*i.e.*, zero polarization) and $\mathbf{R}_f^i(\lambda = 1)$, where $\mathbf{R}_f^i = \mathbf{R}_0^i + \lambda(\mathbf{R}_f^i - \mathbf{R}_0^i)$. The geometry of the \mathbf{R}_f^i and \mathbf{R}_0^i points used in this work are shown

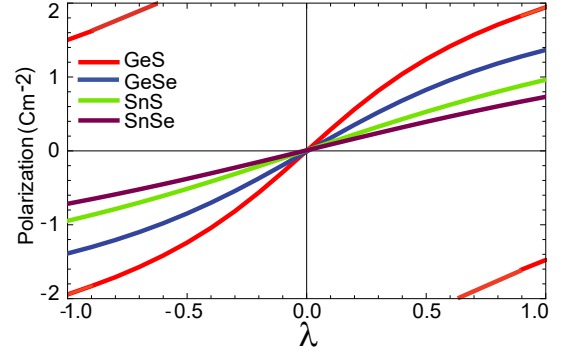


FIG. 9. Electric polarization along a path characterized by different values of λ between the asymmetric ground state $\lambda = \pm 1$ and the centrosymmetric configuration ($\lambda = 0$) on the rectangular unit cell.

in Table II. The polarization calculated at small steps of λ for the different crystals is shown in Fig. 9. Since all points are connected smoothly, the polarization is well-defined and can be calculated as the difference between the polarization at \mathbf{R}_0^i and \mathbf{R}_f^i . The resulting spontaneous polarization values of the different crystals were tabulated in Table. I

TABLE II: Positions (in Bohr) of atoms in single-layer monochalcogenides used to compute the polarization along a path connecting $\mathbf{R}_f^i(\lambda = -1)$ to $\mathbf{R}_f^i(\lambda = 1)$.

GeS

Lattice parameters:
 $\vec{a} = 28.34 \ 0.00 \ 0.00$
 $\vec{b} = 0.00 \ 6.89 \ 0.00$
 $\vec{c} = 0.00 \ 0.00 \ 8.52$

Atom coordinates:

	R_0	$R_f(\lambda = 1.0)$	$R_f(\lambda = -1.0)$
Ge	2.66 1.72 -0.01	2.66 1.72 1.14	2.66 1.72 -1.16

Ge	7.50	5.17	4.25	7.50	5.17	5.41	7.50	5.17	3.09
S	7.09	1.72	-0.01	7.09	1.72	-0.01	7.09	1.72	-0.01
S	3.06	5.17	4.25	3.06	5.17	4.25	3.06	5.17	4.25

GeSe

$$\vec{a} = 28.83 \ 0.00 \ 0.00$$

$$\vec{b} = 0.00 \ 7.50 \ 0.00$$

$$\vec{c} = 0.00 \ 0.00 \ 8.12$$

Atom coordinates:

	R_0	$R_f(\lambda = 1.0)$	$R_f(\lambda = -1.0)$						
Ge	2.98	2.11	0.16	2.98	2.11	0.88	2.98	2.11	-0.55
Ge	7.57	5.86	4.22	7.57	5.86	4.94	7.57	5.86	3.5
Se	7.72	2.11	0.16	7.72	2.11	0.16	7.72	2.11	0.16
Se	2.82	5.86	4.22	2.82	5.86	4.22	2.82	5.86	4.22

SnS

Lattice parameters:

$$\vec{a} = 28.34 \ 0.00 \ 0.00$$

$$\vec{b} = 0.00 \ 7.72 \ 0.00$$

$$\vec{c} = 0.00 \ 0.00 \ 8.12$$

Atom coordinates:

	R_0	$R_f(\lambda = 1.0)$	$R_f(\lambda = -1.0)$						
Sn	2.73	1.93	0.31	2.73	1.93	0.94	2.73	1.93	-0.30
Sn	8.12	5.79	4.37	8.12	5.79	5.00	8.12	5.79	3.75
S	7.60	1.93	0.31	7.60	1.93	0.31	7.60	1.93	0.31
S	3.25	5.79	4.37	3.25	5.79	4.37	3.25	5.79	4.37

SnSe

Lattice parameters:

$$\vec{a} = 28.34 \ 0.00 \ 0.00$$

$$\vec{b} = 0.000 \ 8.11 \ 0.00$$

$$\vec{c} = 0.000 \ 0.00 \ 8.31$$

Atom coordinates:

	R_0	$R_f(\lambda = 1.0)$	$R_f(\lambda = -1.0)$						
Sn	2.98	2.11	0.29	2.98	2.11	0.71	2.98	2.11	-0.13
Sn	8.19	6.16	4.44	8.19	6.16	4.87	8.19	6.16	4.01
Se	8.12	2.11	0.29	8.12	2.11	0.29	8.12	2.11	0.29
Se	3.05	6.17	4.44	3.05	6.17	4.44	3.05	6.17	4.44

The frequency-integral of the injection current tensor for GeSe, GeS, SnS and SnSe monolayers is shown in Fig. 3. It reveals a similar behavior across all materials. Namely, for small values of P the integral is linear, followed by a local minimum (maximum of absolute current) as the polarization increases. Interestingly, the existence of an optimal value of polarization was also found in the frequency-integral of the injection current along the polar axis.

Appendix D: Two-band model for the injection current

We consider a minimal two-band model of GeSe³² with Hamiltonian

$$H = f_0\sigma_0 + f_i\sigma_i, \quad (D1)$$

where $\sigma_i, i = x, y, z$ are the standard Pauli matrices and σ_0 is the 2×2 identity matrix. The functions f_i characterize the onsite potentials and hopping terms. The

Hamiltonian has eigenvectors given by:

$$u_c = A \begin{pmatrix} f_x - if_y \\ \epsilon - f_z \end{pmatrix} \quad (D2)$$

$$u_v = A \begin{pmatrix} f_z - \epsilon \\ f_x + if_y \end{pmatrix}, \quad (D3)$$

where $A^{-2} = 2\epsilon(\epsilon - f_z)$ is the normalization and eigenvalues by $E_{c,v} = f_0 \pm \epsilon$ where $\epsilon = \sqrt{f_i f_i}$ and c, v denote the conduction and valence band respectively. An arbitrary phase factor has been omitted, since the matrix elements in the final expression for η_2 are independent of this phase. The Bloch wave functions are constructed as

$$\psi_{n\mathbf{k}} = \sum_{\mathbf{R}} e^{i\mathbf{k}\cdot\mathbf{R}} [u_{n\mathbf{k}}^A \phi(\mathbf{r} - \mathbf{R}) + e^{i\mathbf{k}\cdot\mathbf{z}_0} u_{n\mathbf{k}}^B \phi(\mathbf{r} - \mathbf{x}_0 - \mathbf{R})], \quad (D4)$$

where u_n^i denotes the eigenvector corresponding to eigenvalue $n = v, c$ (valence and conduction bands) and $i = A, B$ are its first and second components. \mathbf{z}_0 is the position of site B with respect to site A which is taken to be the origin. $\phi(r)$ are s-wave functions and \mathbf{R} runs over all lattice positions. Notice that the phase of the wave function at site B is different than that at site A . We made this choice for consistency with the definition of the Fourier transform in the expression of injection current.¹⁸ The off-diagonal Berry connections give

$$\begin{aligned} r_{cv}^a &= i \langle u_c | \frac{\partial}{\partial k_a} | u_v \rangle \\ &= \frac{i}{2\epsilon(f_x - if_y)} [-(\epsilon + f_z)(\epsilon - f_z)_{,a} \\ &\quad + (f_x - if_y)(f_x + if_y)_{,a}] \end{aligned} \quad (D5)$$

$$\begin{aligned} r_{vc}^a &= i \langle u_v | \frac{\partial}{\partial k_a} | u_c \rangle \\ &= \frac{i}{2\epsilon(f_x + if_y)} [(\epsilon + f_z)(\epsilon - f_z)_{,a} \\ &\quad - (f_x + if_y)(f_x - if_y)_{,a}], \end{aligned} \quad (D6)$$

$$\begin{aligned} r_{vc}^a &= i \langle u_v | \frac{\partial}{\partial k_a} | u_c \rangle \\ &= \frac{i}{2\epsilon(f_x + if_y)} [(\epsilon + f_z)(\epsilon - f_z)_{,a} \\ &\quad - (f_x + if_y)(f_x - if_y)_{,a}], \end{aligned} \quad (D7)$$

where we denote $X_{,a} \equiv \partial X / \partial k_a$. After some calculation, we find the matrix elements

$$r_{cv}^a r_{vc}^b - r_{cv}^b r_{vc}^a = -i\epsilon_{ab} R_{vc}^2, \quad (D8)$$

where R_{vc}^2 is given by

$$R_{vc}^2 = \epsilon_{ab}\epsilon_{ij} \frac{f_{j,b}}{4\epsilon^2} \left[\frac{2(\epsilon - f_z)_{,a} f_i}{(\epsilon - f_z)} - f_{i,a} \right]. \quad (D9)$$

ϵ_{ab} is the Levi-Civita symbol in 2D. The injection current is then

$$\eta_2^{yyz} = \frac{-ie^3\pi}{\hbar^2} \frac{1}{V} \sum_{\mathbf{k}} \epsilon_{,y} R_{vc}^2 \delta(2\epsilon - \hbar\omega), \quad (D10)$$

where V is the 2D volume of the sample. To obtain a bulk value we divide by the thickness of the slab d . For the model in Fig. 4, the f_i functions are $f_x - if_y = e^{i\mathbf{k}\cdot\mathbf{x}_0}(t_1 + te^{-i\mathbf{k}\cdot\mathbf{a}_1} + t_2e^{-i\mathbf{k}\cdot(\mathbf{a}_1+\mathbf{a}_2)} + te^{-i\mathbf{k}\cdot\mathbf{a}_2})$, $f_z = \bar{\Delta}$.

We defined $\bar{\Delta} = \Delta - (t_{AA} - t_{BB})[\cos \mathbf{k} \cdot \mathbf{a}_1 + \cos \mathbf{k} \cdot \mathbf{a}_2]$ and $f_0 = \Delta_r = (t_{AA} + t_{BB})[\cos \mathbf{k} \cdot \mathbf{a}_1 + \cos \mathbf{k} \cdot \mathbf{a}_2]$. Δ is the onsite potential, t, t_1, t_2 the nearest neighbors and t_{AA}, t_{BB} the next to nearest neighbors. In simulations, we take $z_0 = a$, *i.e.*, a square lattice with lattice constant a .

-
- ¹ B. I. Sturman and P. J. Sturman, *Photovoltaic and Photo-refractive Effects in Noncentrosymmetric Materials* (CRC Press, 1992).
- ² J. E. Spanier, V. M. Fridkin, A. M. Rappe, A. R. Akbashaev, A. Polemi, Y. Qi, Z. Gu, S. M. Young, C. J. Hawley, D. Imbrenda, G. Xiao, A. L. Bennett-Jackson, and C. L. Johnson, *Nat. Photonics* **10**, 611 (2016).
- ³ N. Laman, A. I. Shkrebtii, J. E. Sipe, and H. M. van Driel, *Applied Physics Letters* **75**, 2581 (1999).
- ⁴ E. Luppi, , and V. Veniard, *Semicond. Sci. Technol.* **31**, 123002 (2016).
- ⁵ K. Kushnir, M. Wang, P. D. Fitzgerald, K. J. Koski, and L. V. Titova, *ACS Energy Letters* **2**, 1429 (2017).
- ⁶ T. Rangel, B. M. Fregoso, B. S. Mendoza, T. Morimoto, J. E. Moore, and J. B. Neaton, *Phys. Rev. Lett.* **119**, 067402 (2017).
- ⁷ S. R. Panday and B. M. Fregoso, *Journal of Physics: Condensed Matter* **29**, 43LT01 (2017).
- ⁸ H. Wang and X. Qian, *Nano Letters* **17**, 5027 (2017).
- ⁹ K. Chang, J. Liu, H. Lin, N. Wang, K. Zhao, A. Zhang, F. Jin, Y. Zhong, X. Hu, W. Duan, Q. Zhang, L. Fu, Q.-K. Xue, X. Chen, and S.-H. Ji, *Science* **353**, 274 (2016).
- ¹⁰ M. Mehboudi, B. M. Fregoso, Y. Yang, W. Zhu, A. van der Zande, J. Ferrer, L. Bellaiche, P. Kumar, and S. Barraza-Lopez, *Phys. Rev. Lett.* **117**, 246802 (2016).
- ¹¹ S. Barraza-Lopez, T. P. Kaloni, S. P. Poudel, and P. Kumar, *Phys. Rev. B* **97**, 024110 (2018).
- ¹² L. Z. Tan, F. Zheng, S. M. Young, F. Wang, S. Liu, and A. M. Rappe, *Npj Computational Materials* (2016).
- ¹³ B. M. Fregoso, T. Morimoto, and J. E. Moore, *Phys. Rev. B* **96**, 075421 (2017).
- ¹⁴ X. Gonze *et al.*, *Computer Physics Communications* **180**, 2582 (2009).
- ¹⁵ J. P. Perdew, K. Burke, and Y. Wang, *Phys. Rev. B* **54**, 16533 (1996).
- ¹⁶ C. Hartwigsen, S. Goedecker, and J. Hutter, *Phys. Rev. B* **58**, 3641 (1998).
- ¹⁷ TINIBA is a tool written in bash, perl, and fortran to compute optical responses based on the ABINIT. <https://github.com/bemese/tiniba>.
- ¹⁸ J. E. Sipe and A. I. Shkrebtii, *Phys. Rev. B* **61**, 5337 (2000).
- ¹⁹ P. E. Blöchl, O. Jepsen, and O. K. Andersen, *Phys. Rev. B* **49**, 16223 (1994).
- ²⁰ L. C. Gomes and A. Carvalho, *Phys. Rev. B* **92**, 085406 (2015).
- ²¹ R. D. King-Smith and D. Vanderbilt, *Phys. Rev. B* **47**, 1651 (1993).
- ²² R. Resta, *Rev. Mod. Phys.* (1994).
- ²³ R. Fei, W. Kang, and L. Yang, *Phys. Rev. Lett.* **117**, 097601 (2016).
- ²⁴ N. Laman, M. Bieler, and H. M. van Driel, *Journal of Applied Physics* **98**, 103507 (2005).
- ²⁵ M. Bieler, N. Laman, H. M. van Driel, and A. L. Smirl, *Applied Physics Letters* **86**, 061102 (2005).
- ²⁶ D. Sun, C. Divin, J. Rioux, J. E. Sipe, C. Berger, W. A. de Heer, P. N. First, and T. B. Norris, *Nano Letters* **10**, 1293 (2010).
- ²⁷ D. A. Bas, K. Vargas-Velez, S. Babakiray, T. A. Johnson, P. Borisov, T. D. Stanescu, D. Lederman, and A. D. Bristow, *Applied Physics Letters* **106**, 041109 (2015).
- ²⁸ D. A. Bas, R. A. Muniz, S. Babakiray, D. Lederman, J. E. Sipe, and A. D. Bristow, *Opt. Express* **24**, 23583 (2016).
- ²⁹ G. Li, K. Kushnir, M. Wang, Y. Dong, S. Chertopalov, A. M. Rao, V. N. Mochalin, R. Podila, K. Koski, and L. V. Titova, in *2018 43rd International Conference on Infrared, Millimeter, and Terahertz Waves (IRMMW-THz)* (2018).
- ³⁰ M. Pagliaro, G. Palmisano, and R. Ciriminna, *Flexible Solar Cells* (John Wiley & Sons, Ltd, 2008).
- ³¹ A. K. Singh and R. G. Hennig, *Applied Physics Letters* (2014).
- ³² A. M. Cook, B. M. Fregoso, F. de Juan, S. Coh, and J. E. Moore, *Nature Communications* **8**, 14176 (2017).